Desalination and Water Treatment
www.deswater.com

doi: 10.5004/dwt.2021.27396

230 (2021) 240–251
August

Adsorption–desorption of tetracycline onto molecularly imprinted polymer: isotherm, kinetics, and thermodynamics studies

Aram Dokht Khatibi[a], Amir Hossein Mahvi[b], Nezamaddin Mengelizadeh[c], Davoud Balarak[a,*]

[a]*Department of Environmental Health, Health Promotion Research Center, Zahedan University of Medical Sciences, Zahedan, Iran, emails: dbalarak2@gmail.com (D. Balarak), dbchemistry2@gmail.com (A.D. Khatibi)*
[b]*Center for Solid Waste Research, Institute for Environmental Research, Tehran University of Medical Sciences, Tehran, Iran, email: ahmahvii@gmail.com*
[c]*Research Center of Health, Safety and Environment, Department of Environmental Health Engineering, Evaz Faculty of Health, Larestan University of Medical Sciences, Larestan, Iran, email: Nezammengelizadeh@gmail.com*

Received 19 January 2021; Accepted 5 May 2021

ABSTRACT

Molecularly imprinted polymer (MIP) was obtained by the bulk polymerization method. The MIP was characterized by different spectroscopic techniques like a TGA, SEM, and N_2 adsorption–desorption and pH_{PZC}. The adsorption of tetracycline (TC) onto MIP from solution was studied, in which the influence of pH, initial TC concentration, MIP mass, temperature, and contact time were investigated. The surface area of MIP was 172.9 m^2/g the highest removal efficiency was obtained at a pH of 5, MIP dose of 0.6 g/L, TC concentration of 25 mg/L, the temperature of 50°C, and reaction time of 60 min°C. The adsorption kinetic was explored and best represented by the pseudo-second-order kinetic model and the adsorption isotherm experimental data had the best fitness with the Langmuir model, suggesting that homogeneous uptake was the principal mechanism adopted in the process of TC adsorption. The maximum adsorption capacity based on the Langmuir model was 416.5, 476.2, 588.3, and 666.5 mg/g at temperatures of 20°C, 30°C, 40°C, and 50°C, respectively. The thermodynamics of the adsorption indicated the endothermic and spontaneous nature of the process. The usability after six cycles was approved so that the adsorption capacities were associated with insignificant reduction (from 153.4 (92.04%) to 140.6 mg/g (84.38)) after the employed cycles.

Keywords: Molecularly imprinted polymer; Tetracycline; Kinetics; Isotherm; Thermodynamics

1. Introduction

Utilization of antibiotics for medical purpose are widely increased as well as are used in animal feeds because of disease prevention and stimulate growth [1,2]. Therefore, a major concern that has recently been raised is associated with antibiotics in water bodies [3,4]. Even at low concentrations, antibiotics could lead to creating an adverse effect on ecosystems and human beings due to bioaccumulation, chronic and acute effects, high water solubility, high persistent, bioactivity, and string effects on microbial resistance and community [5,6].

Tetracycline (TC) with a chemical formula of ($C_{22}H_{24}N_2O_8$) has been extremely applied in human cure and livestock therapy as well as the agricultural industry [7,8]. This type of antibiotics could be used for bacterial infections like gonorrhea, acne, and infections of the urinary tract [9,10]. TC with widespread use has been classified as an emerging pollutant and caught increasing concern [11]. The existence of antibiotics in the environment can lead to adverse

---

* Corresponding author.

influences on microorganisms and the development of resistant pathogens, and further, be hazardous to human health [12,13]. The removal of residual TC from the wastewater before release to the environment is necessary.

The pollution of aquatic bodies by drugs discharged from various activities in the Pharmaceutical industries is a global environmental challenge that must be resolved [14]. Most of these industries in third-world nations make little or no provision to treat their effluent before discharging it [15,16].

Many treatment methods have been taken to eliminate antibiotics from aqueous solutions such as biological treatment, electrochemical process, coagulation–precipitation, ion-exchange, adsorption, membrane process, and photocatalysts [17,18]. It appears that the common biological methods could not sufficiently remove pharmaceutical compounds [19]. Due to the concentration of TC antibiotics at mg/L level in wastewater, the adsorption is appropriate for the remediation of the polluted water containing the low concentration of the pollutants [20,21]. Adsorption technique among others is identified as the commonest method used in the decontamination of antibiotics in discharged effluents [22]. Some of its economic and technological advantages are, it is cheap and easy to operate, accessible and available, profitable and efficient, and effective than other techniques [23].

Because of the complexity of environmental samples, molecularly imprinted polymers (MIPs) have been recently established for enhancing the selectivity of analytical methods [24]. The designing MIPs is in such a way that can improve their selectivity for a special structure. These polymers have various applications [25]. Producing the MIP is including the polymerization of suitable functional monomer and cross-linker in the presence of a template molecule, which is carrying out by an initiator [26]. The template is finally rinsed by an appropriate solvent for creating the cavities in the polymer [24]. The various cases, that is, ease of preparation, stability at extremes of pH and temperature, high selectivity, and low operational cost are considered as the advantages of MIPs. The mentioned advantages have provoked the researchers to define different applications, for example, their employment in adsorption and extraction of pharmaceuticals [27]. The application of MIPs for the extraction of pharmaceuticals has been previously studied; for instance, it has been employed for selective extraction of antiviral and non-steroid anti-inflammatory pharmaceuticals [28].

MIP, as a useful adsorbent material, has played a crucial role in the decontamination of antibiotics in an aqueous environment. Its usage as an adsorbent comes with many advantages such as high renewable, very good affinity, non-toxic and it can be regenerated at a very low cost. This material is available in large quantity and also has a high surface area [24,25].

The objective of this work is to investigate the potential and adsorption efficiency of MIP for the removal of TC from aqueous solutions. The MIP was characterized in terms of surface areas and morphology. The effects of operational parameters such as pH, amount of MIP, initial TC concentration, temperature, and contact time on the adsorption of TC onto MIP were analyzed to determine the factors controlling the rate of adsorption. Langmuir, Freundlich, Temkin, and Dubinin–Radushkevich (D–R) isotherm models were studied to understand the adsorption process. Kinetic studies were also evaluated using pseudo-first-order (PFO), pseudo-second-order (PSO), and intraparticle diffusion (IPD). Thermodynamic parameters were also determined.

2. Materials and methods

2.1. Chemicals and reagents

Analytical grade TC (formula: $C_{22}H_{24}N_2O_8$, molar mass: 444.4 g/mol) was used in this research for the preparation of TC solution used for experimental adsorption and were obtained from Sigma-Aldrich (USA). A stock solution containing 1,000 mg/L was prepared by dissolving 1 g of analytical grade TC with distilled water in a 1 L standard flask. TC solution of different initial concentrations (10–100 mg/L) were obtained by diluting stock solution. All chemicals and reagents such as NaH_2PO_4, orthophosphoric acid, pyrrole, iron(III) chloride, $NaNO_3$, methanol, and HCl and NaOH were obtained from Merck Company (Germany). The chemical structure of TC was represented in Fig. 1.

2.2. Batch adsorption technique

Batch adsorption techniques were performed to study the consequence of limitations such as MIP mass, initial TC concentration, contact time, solution pH, and temperature for the exclusion of TC by MIP. Stock solutions of TC (1,000 mg/L) were prepared by dissolving an accurate quantity of TC individuals. Deionized water was used in preparing the stock solutions and also throughout the experimental analysis.

The process was approved by shaking 100 mL conical flasks containing 0.6 g of MIP and 50 mL of TC solutions of anticipated concentration with attuned pH using a shaker water bath at a continuous speed of 180 rpm. To observe the effect of adsorbent dose on TC adsorption, different amounts of MIP (varying from 0.1 to 1 g/L) were, respectively, added into the initial concentration of TC (100 mg/L) at 30°C and the desired pH until the equilibrium time was reached. By varying the pH from 3 to 11, the effect of pH on TC adsorption was

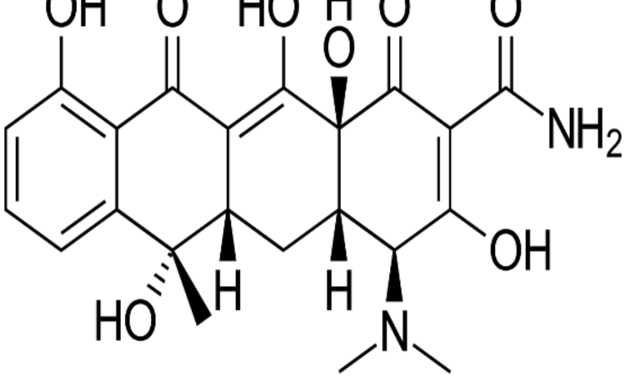

Fig. 1. Structure of TC.

studied and modified to the desired value using 0.1 mol/L HCl and 0.1 mol/L NaOH solutions. The supernatant solution was separated from the adsorbent by a centrifuge at 3,000 rpm for 5 min at the end of the adsorption cycle. High-performance liquid chromatography (HPLC; Agilent, USA, 1260 Infinity II) with UV/vis CE 4900 as a detector was used for the analysis of TC concentration column (Germany), C18 (250 mm × 4.6 mm) was used in this way. The volume of injection and wavelength of measurement was 20 μL and 288 nm. The orthophosphoric (65%) and buffer 96.65% (NaH_2PO_4) were applied as a mobile phase. Eq. (1) was used to measure the percentage of TC removal (R) [29]:

$$\%R = \left(\frac{C_0 - C_e}{C_0}\right) \times 100 \tag{1}$$

where C_0 (mg/L) and C_e (mg/L) are TC concentrations initially and at time t, respectively.

For the adsorption process, TC solutions of different concentrations (25–100 mg/L) for TC were agitated with 0.6 g of MIP until the equilibrium was achieved. Equilibrium adsorption capacity, q_e (mg TC per g MIP) was designed from Eq. (2) [30]:

$$q_e = \frac{V\left(C_0 - C_e\right)}{W} \tag{2}$$

where V (L) is the volume of solution and W (g) is the weight of MIP.

pH_{PZC} is determined to detect the type of interactions, which occur between MIP and charged soluble species; the procedure of its determination is described as follows: first, we prepared a stock solution of 0.1 M $NaNO_3$ using distilled water. After that, this solution was employed to prepare ten different solutions with pH values (2–11); the adjustment of the pH of these solutions has been carried out using either 0.1 mol/L HCl and 0.1 mol/L NaOH. We then poured 0.1 g MIP in 50 mL of each solution and left them to being stirred for 24 h. Lastly, we measured the final pH and plotted it as a function of the initial pH of the solution.

2.3. Synthesis of polymers

The MIP was obtained as the process described by Cromack and the bulk polymerization method [31]. One 300 mg or mmol of the template and 4 mmol of pyrrole were dissolved in 40 mL of a solution containing 3 volumes of methanol and 2 volumes of water. The resulting solution was stirred for half an hour. 9.2 mmol of iron(III) chloride was added to the solution as an oxidizer and stirred for another half an hour. The polymerization was then finalized in an argon atmosphere (oxygen plays a strong inhibitory role in the polymerization process) without stirring for 72 h. The obtained MIP was washed using a vacuum system, filtered, and then washed with distilled water to remove residual iron and other impurities and dried at room temperature. Non-imprinted polymer (NIP) was synthesized similarly to the above method without the presence of the target molecule. The obtained MIP was completely ground and milled by a mortar. The target molecule was completely removed and extracted by the Soxhlet process in methanol. To ensure complete removal of the template, the solution inside the balloon was sampled and analyzed by HPLC during Soxhlet. After complete removal of the template, the mixture was filtered and dried in a vacuum oven at 70°C.

The characterization of the MIP and NIP was tested by a scanning electron microscopy (SEM), X-ray diffraction (XRD), and thermogravimetric (TGA) analysis. The specific surface areas of the MIP and NIP were measured by N_2 adsorption–desorption at 77 K and determined by Brunauer–Emmett–Teller (BET) method.

3. Results and discussion

3.1. MIP characterization

This phenomenon was further confirmed by the data of specific surface areas obtained from the BET method. The specific surface areas of the MIP and NIP were calculated to be 172.9 and 97.2 m^2/g. The specific surface areas of the MIP were identified to be almost 1.8 times compared to the NIP. It may be accredited to the fact that MIP has a template during synthesis, and the template is removed during its washing. Washing of the MIPs is led to removing the template from the surface of the pores however this process has not occurred for NIP; this resulted in enhancing the surface area of the MIP. This facilitates the adsorption of the antibiotic on the MIP surface. Since the pore diameter of both MIP and NIP is higher than 50 nm, their surface is macro-porous. The pore volume for MIP and NIP were obtained at 0.276 and 0.241 cm^3/g, respectively.

The morphology of synthesized polymer was surveyed using the results of SEM. According to the results of this analysis provided in Fig. 2, MIP has a rougher surface in comparison with the NIP (it has a smooth surface); this results in providing a higher surface area for adsorption. The difference in morphology spotted in the image of MIP, compared to NIP, may be described by the presence of a template during the synthesis of the polymer and its washing.

The thermal stability of the polymer was estimated using TGA analysis, and the results of this analysis are publicized in Fig. 3. This Fig. 3 highlights the lack of weight loss in polymer by increasing the temperature of 100°C–300°C. While increasing the temperature to values higher than the mentioned range will lead to rapid decomposition of polymer, which may be related to the structural difference created during removal of the template. The occurrence of a rapid weight loss has been detected at temperatures range of 350°C–500°C. Moreover, Fig. 3 indicates that, at a temperature higher than 500°C, the polymer is absolutely decomposed. According to the above, good thermal stability for synthesized polymer could be observed at temperatures lower than 300°C.

To acquire information on the crystallinity of the homogenized powder sample, the XRD result (Fig. 4) can be valuable. Considering the results represented in

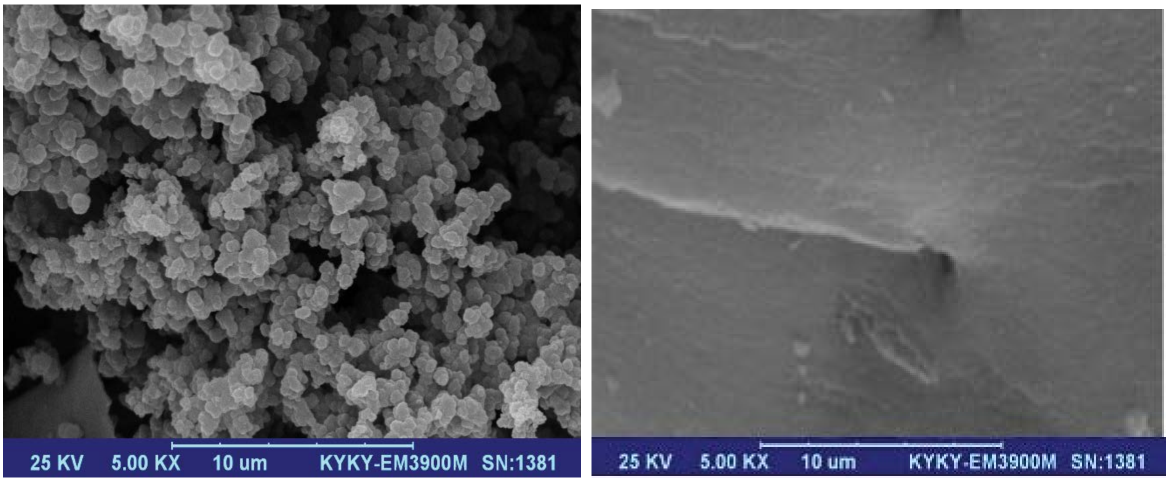

Fig. 2. SEM image of MIP and NIP.

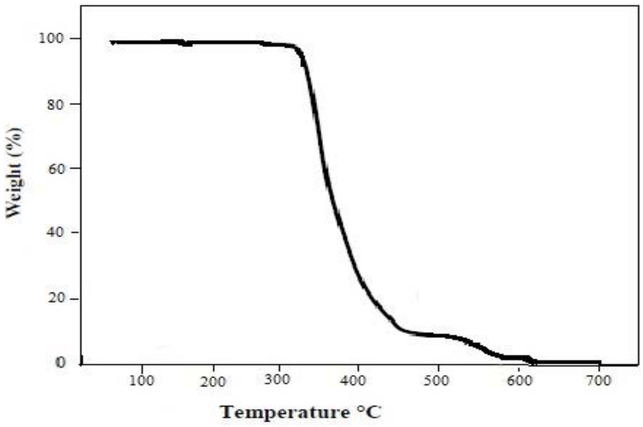

Fig. 3. TGA curve of the MIP.

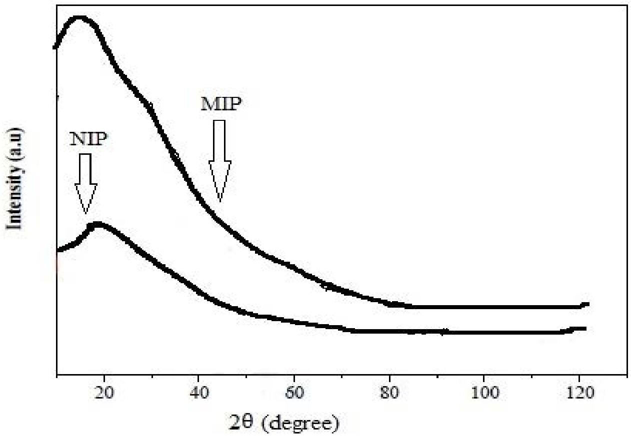

Fig. 4. XRD curve of the MIP and NIP.

Fig. 4, the similarity in the pattern of MIP and NIP can be detected; this signposts that there is the same structural backbone in their structure. Moreover, the XRD peak could not provide any evidence for the absence of crystallinity and the amorphous nature of the polymer. This result was observed to be in agreement with the results of a similar study [32].

3.2. Effect of MIP weight

As mentioned before, MIP used in the present wastewater treatment survey to study the effect of weights in the removal % of TC from the aqueous solution. Various weights including 0.01, 0.02, 0.03, 0.04, 0.05, 0.06, 0.07, 0.08, 0.09, and 0.1 g of MIP used in batch adsorptive removal experiments in 100 ml aqueous solutions containing 100 mg/L of TC (Fig. 5). The pH of the solutions was kept at 7. The obvious obtained result of the parameter was that as the adsorbent weight in the contaminated solution was increased, the TC concentration of the solutions was decreased. So the obtained removal % was enhanced. This is due to the fact that adding more amount of adsorbent in solution provides more surface area for

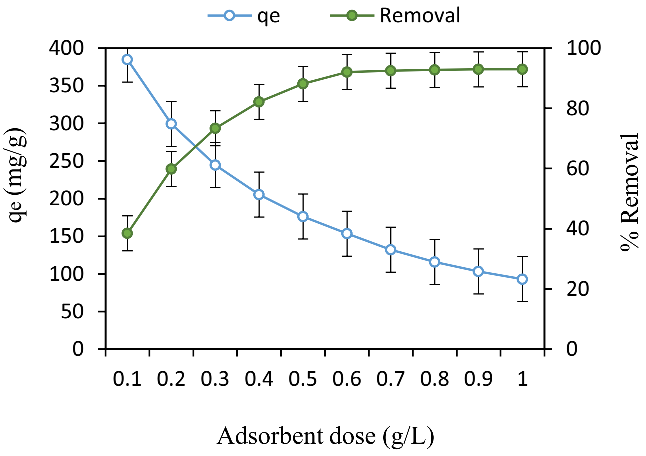

Fig. 5. Effect of MIP dosage on TC adsorption onto MIP (C_0 = 100 mg/L, time = 60 min, pH = 5, and temperature = 30°C ± 2°C).

the adsorption of the pollutant and consequently the removal % is enhanced [33]. This phenomenon is observable until a weight that the system reaches an equilibrium. So adding an extra amount of adsorbent will not be efficient for increasing the removal %. According to the performed experiments, the optimum amount of MIP was turned out to be 0.6 g.

3.3. Effect of pH and determination of point of zero charge

TC is a hydrophilic amphiphilic molecule with a variety of functional groups, and there are three ionization equilibrium constants in an aqueous solution, namely $pK_1 = 3.30$, $pK_2 = 7.68$, and $pK_3 = 9.68$ [34]. Therefore, under different pH conditions, TC can be dissociated into four different forms, namely TC^+, TC^0, TC^-, and TC^{2-}. The effect of the solution pH on the adsorption capacity is shown in Fig. 6. The results show that the adsorption capacities of MIP were higher when the pH of the solution was neutral, but the adsorption capacities of MIP were lower under the condition of strong alkalinity [35].

MIP pH_{PZC} was originated to be 7.2 (Fig. 7). When the pH of the solution is less than that of the adsorbent pHpzc, the adsorbent will be protonated and positively charged and easily adsorb negatively charged substances. In contrast, when the pH of the solution is greater than that of the adsorbent pHpzc, the polar functional groups of the adsorbent will be dissociated and negatively charged [36]. However, TC exists in the form of TC^+ under acidic conditions and TC^- and TC^{2-} under alkaline conditions. Therefore, the adsorption performance of the adsorbent decreased under the action of electrostatic repulsion. When the pH was between 5 and 7, the primary existence form of TC was TC^0 with almost no charge. Therefore, the change in pH had little impact on the adsorption performance. In this range, the adsorption amount was large, indicating that there were non-electrostatic interactions such as π–π accumulation and hydrogen bonding between the MIP and the TC [37].

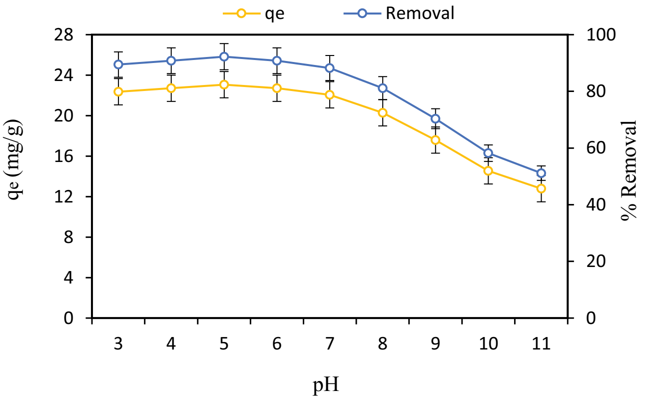

Fig. 6. Effect of initial pH on the adsorption of TC (C_0 = 100 mg/L, time = 60 min, MIP mass = 0.6 g/L, and temperature = 30°C ± 2°C).

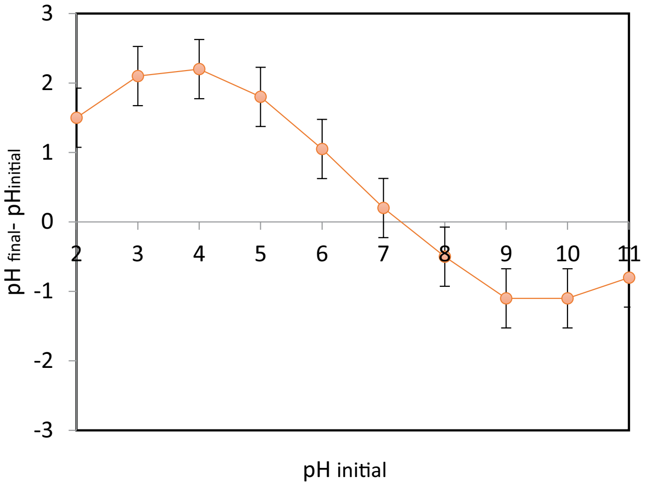

Fig. 7. Determination of the point of zero charge of MIP.

3.4. Equilibrium studies

It provides fundamental information on the adsorption mechanism, surface properties, and the affinity of adsorbents, which helps to determine the application of adsorption as a unit operation [37]. The results obtained on the adsorption of TC onto MIP were tested by different isotherm models as follows.

3.4.1. Langmuir model

This model assumes that the adsorption occurs at specific homogenous active sites on the adsorbent. These active sites have an affinity for adsorption of a monolayer and there is no interaction between adsorbed molecules. The linear form of Langmuir equation is expressed as [38,39]:

$$\frac{C_e}{q_e} = \frac{1}{k_L q_m} + \frac{C_e}{q_m} \tag{3}$$

where q_e is the amount of TC adsorbed and has the units of mg/g, q_m is the maximum holding power of the MIP when the adsorbent superficial layer is saturated by the adsorbate which has the units of mg/g and k_L is a constant related to the Langmuir equilibrium, k_L is dependent on the adsorbed energy and has the units of L/mg and the plot of C_e/q_e vs. C_e (Fig. 8a) gives a straight line in which $1/q_{\max}$ and k_L are computed.

3.4.2. Freundlich isotherm

Freundlich isotherm assumes that the adsorption of the adsorbate toward the adsorbent is through the multiple surfaces located at both the interior and exterior layers of the adsorbent which is generally referred to as a heterogeneous distribution, the linear form of the Freundlich isotherm is [40]:

$$\log q_e = \log K_F + \frac{1}{n} \ln C_e \tag{4}$$

where q_e is the adsorbed amount and has the units of mg/g, K_F ((L/mg/)$^{1/n}$) is the Freundlich isotherms constant,

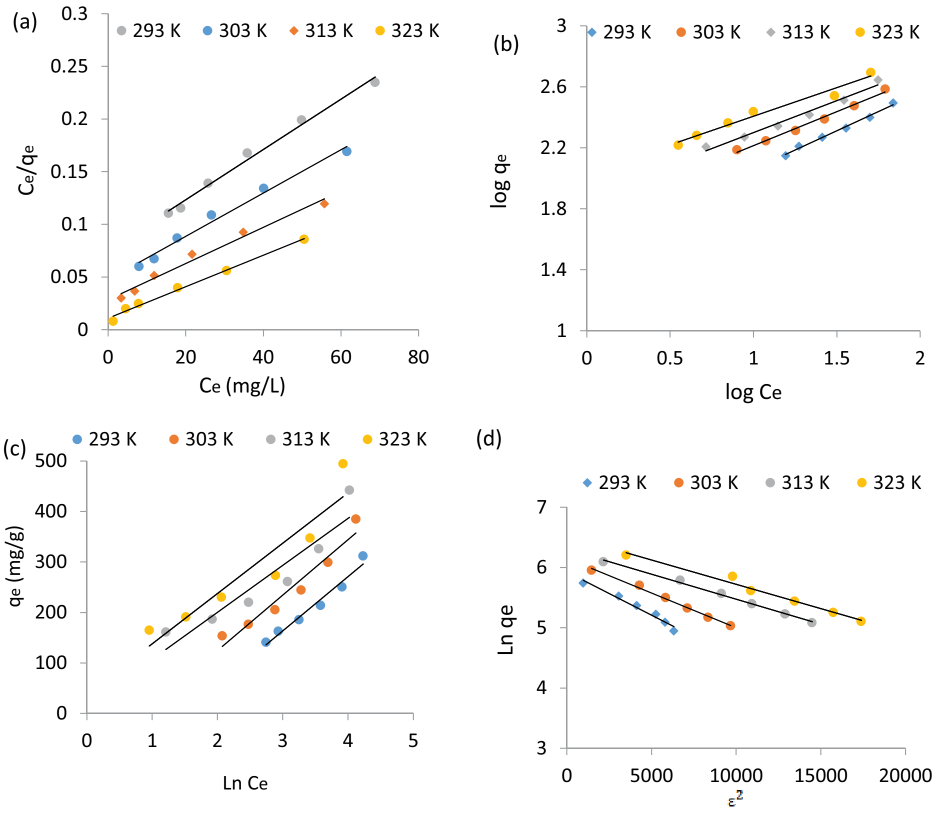

Fig. 8. Adsorption isotherms for TC removal by MIP: (a) Langmuir, (b) Freundlich, (c) Temkin, and (d) D–R.

and $1/n$ is a function of the potential of the adsorbate to adhere to the adsorbent surfaces, a plot of $\log q_e$ vs. $\log C_e$ (Fig. 8b) is plotted in which the values of $1/n$ and K_F are computed from slopes and intercepts, respectively.

3.4.3. Temkin isotherm

Temkin adsorption isotherms are based on the assumption that the heat of adsorption decreases with reference to the increase in adsorbent coverage. The linear form of Temkin isotherm is [41]:

$$q_e = B\ln A + B\ln C_e \tag{5}$$

where $B = (RT/b)$, b is Temkin constant which is linked to the heat of sorption, A is Temkin isotherm constant, T is the absolute temperature in kelvins, and R is the molar gas constant and a plot of q_e vs. $\ln C_e$ (Fig. 8c) was drawn and the values of B and A were computed from slopes and intercepts, respectively.

3.4.4. D–R isotherm

The D–R model is expressed as Eq. (6) [42]:

$$\ln q_e = \ln q_m - K\varepsilon^2 \tag{6}$$

where K indicates the adsorption energy constant, q_m represents the theoretical saturation capacity (mg/g), and ε is the Polanyi potential, calculated from Eq. (7) [43]:

$$\varepsilon = RT\ln\left(1+\frac{1}{C_{\text{eq}}}\right) \tag{7}$$

where C_{eq} (mol/L) is the equilibrium concentration of adsorbate. The constant K is expressed by the slope of the plot of $\ln q_e$ vs. ε^2 (Fig. 8d), and the adsorption capacity, q_m (mg/g) was represented by the intercept.

The mean free energy of adsorption, E (kJ/mol), was calculated using Eq. (10) [44]:

$$E = -\left(2K\right)^{-1/2} \tag{8}$$

From the comparison of the regression coefficients it was found that Langmuir > D–R > Freundlich > Temkin (Table 1 and Figs. 8a–d). On the basis of the comparison of q_e values calculated, there was an insignificant disparity between q_e values from the Langmuir model and the experimental values, whereas there was an obvious gap of q_e values from D–R model with the experimental values, illustrating that Langmuir fits better than D–R model. Therefore, adsorption of TC using MIP can best be described by the Langmuir model and consequently an indication that single layer adsorption was predominant.

The value of E calculated using above Eq. (9) at low temperatures is less than 8 and this implies that the type of adsorption involved in this study is physiosorption (physical sorption), but at higher temperatures the value of E increases to higher than 8 and the adsorption is chemical.

The adsorption capacity (q_m) values of various adsorbents and MIP were compared for TC adsorption. There are significant differences between the q_m values of different adsorbents as shown in Table 2. The results in Table 2 show that MIP has an average good ability to adsorb TC from an aqueous solution.

3.5. TC adsorption kinetics

The investigation of kinetic data is extremely relevant to the adsorption operation by providing information on the possibility of applying a particular adsorbent, the time required for the process to reach equilibrium, the mass transfer parameters, and about adsorption rate. The kinetic behavior of TC adsorption on MIP was evaluated employing

Table 1
Isotherm parameters for adsorption of TC onto MIP at various temperatures

Temperature (K)	Freundlich			Langmuir			
	K_F	n	R^2	q_m	R_L	K	R^2
293	35.85	1.981	0.953	416.5	0.847	0.0018	0.994
303	58.61	2.242	0.965	476.2	0.914	0.00094	0.996
313	75.94	2.386	0.977	588.3	0.944	0.00059	0.998
323	107.5	2.665	0.9712	666.5	0.965	0.00036	0.997
Temperature (K)	Temkin			D–R			
	B	A	R^2	q_m	K	E	R^2
293	107.5	13.61	0.921	256.5	0.024	4.56	0.982
303	109.8	11.51	0.946	327.4	0.019	5.12	0.988
313	93.08	3.158	0.877	396.3	0.011	6.74	0.991
323	99.69	1.964	0.874	425.4	0.007	8.45	0.989

Table 2
Comparison of the maximum adsorption of various adsorbent for TC

Adsorbent	Experimental conditions				Thermodynamic	q_e (mg/L)	Ref.
	pH	C_0 (mg/L)	Dose (g/L)	Time (min)			
MIP	7	100	0.6	60	Endothermic-spontaneous	293 = 416.5 303 = 476.2 313 = 588.3 323 = 666.5	This study
Grapheme oxide magnetic	5.7	200	1.5	90	Endothermic-spontaneous	440	35
Iris tectorum-AC	5	200	2	120	Endothermic-spontaneous	455	36
Macadamia nut-AC	7.0	250	1.2	90	Endothermic-spontaneous	525	13
Grape processing waste-AC	5.7	200	1	80	Endothermic-spontaneous	313	37
Graphene oxide	6.2	167	1.2	60	Endothermic-spontaneous	340	38
SWCNT	5.7	100	0.8	120	Exothermic-spontaneous	100	39
MWCNT	6	90	0.8	120	Endothermic-spontaneous	375	39
Sorbo commercial AC	4	100	1.2	180	Exothermic-spontaneous	471	40
Smectite	6	100	1.5	240	Endothermic-spontaneous	462	41
Kaolinite	7	100	2	180	Exothermic-spontaneous	4.7	43
Rectorite	6	50	2	240	Endothermic-spontaneous	140	44
Palygorskite	8	50	1.2	180	Exothermic-spontaneous	99.2	45
Mesoporous silica	7	100	2	240	Endothermic-spontaneous	85.5	9
Cu-13X	7	100	2	180	Endothermic-spontaneous	39.5	10
Zero-valent iron	6.5	50	1.2	240	Exothermic-spontaneous	35.8	11
Apricot nut shells-AC	6	50	2	180	Endothermic-spontaneous	51.4	46
Maize stalks	7	100	.5	150	Endothermic-spontaneous	41.3	7
Azolla filiculoides	6	100	4	120	Endothermic-spontaneous	29.4	8
Pyrolysis char-AC	7	100	2	180	Endothermic-spontaneous	48.2	12

adsorption capacity curves (q_t) as a function of contact time (t) varying between 10 and 120 min, for different initial TC concentrations. The kinetic profile is illustrated in Fig. 9. As shown in Fig. 9, at the initial stage adsorption capacity show a rapid increase with time up to saturation capacity at 30 min, after that, the adsorption capacity became slow and significantly constant at 60 min. Rapid increase at the onset of the adsorption process may be attributed to high solute concentration gradient as well as vacant pore voids [45]. However, the contact time increased and adsorption capacity slows down, this is because the available adsorption sites is been occupied [46]. The movement of TC into the pore surface will be slow due to the few sites available; this will continue until equilibrium is achieved.

Different adsorption kinetics models such as PFO, PSO, and IPD kinetic model were used for reviewing the kinetics models that best fit with the adsorption of TC onto MIP adsorbents. Eqs. (9)–(11) in order to represent the PFO, PSO kinetics model, and IPD model, respectively [47–49].

$$\log\left(q_e - q_t\right) = \log q_e - \frac{K_1}{2.303}t \tag{9}$$

$$\frac{t}{q_t} = \frac{1}{K_2 q_e^2} + \frac{t}{q_e} \tag{10}$$

$$q_t = K_3 t^{1/2} + I \tag{11}$$

where K_1 represents the PFO rate constant, K_2 is the PSO rate constant, and K_3 represents the IPD propagation rate constant. I is a constant and is associated with the thickness of the boundary layer.

The rate constants and the correlation coefficients were calculated and summarized in Table 3. The value of the correlation coefficient R^2 for the PSO adsorption model was relatively high (>0.993) at all concentrations. Also, q_e (calculated) using the PSO model is equal to that obtained experimentally. These values indicated that adsorption follows the PSO mechanism. Also, the plot (Fig. 10) of t/q_t vs. t for PSO showed a linear relationship between t/q_t and t.

The theoretical adsorption capacities predicted by the PSO model were 46.9 mg/g (25 mg/L), 93.45 mg/g (50 mg/L), 136.9 mg/g (75 mg/L), 185.1 mg/g (100 mg/L), and agreed well with the experimental values. Similar to that observed in Table 3, it can be highlighted that the theoretical capacities increased with the increase of the initial concentration, confirming that the TC adsorption capacity was favored in higher concentrations.

The IPD model was usually used to assess the diffusion mechanism during the adsorption kinetic process. The fitting curves of the IPD model for TC occurred in two linear steps (Fig. 11 and Table 3), illustrating that the diffusion mechanism of this process could be described as two separate stages. The first sharp stage through a transfer of the antibiotics from the solution to the surface of sorbent was caused by the interactions between the antibiotics and the active binding sites of the MIP, and by the formation of the external surface transport

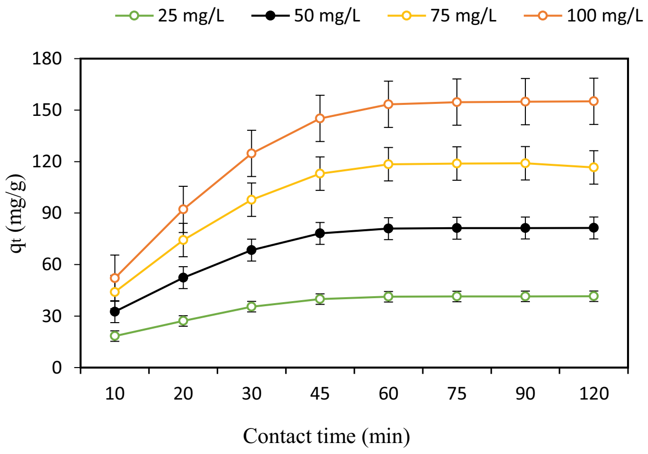

Fig. 9. Effect of contact time on TC removal (pH = 6, MIP mass 0.6 g/L, and temperature = 30°C ± 2°C).

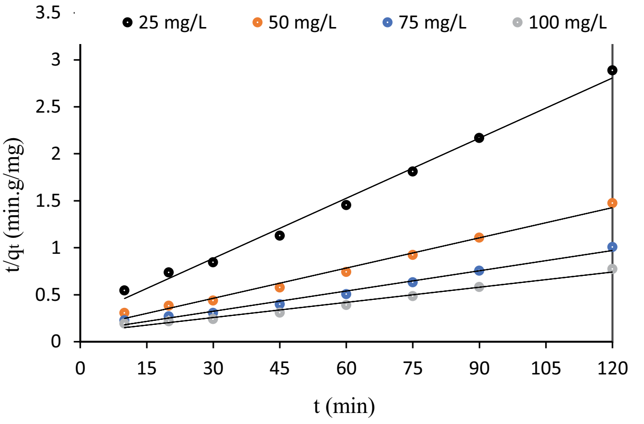

Fig. 10. Pseudo-second-order kinetic plots for adsorption of TC on MIP.

Table 3
Values of kinetic parameters for the adsorption of TC onto MIP

		IPD model			PFO			PSO		
	$q_{e,\mathrm{exp}}$	K_3	I	R^2	$q_{e,\mathrm{cal}}$	K_1	R^2	$q_{e,\mathrm{cal}}$	K_2	R^2
25	41.55	2/84	15/64	0/567	15/56	0/044	0.895	46/9	0/001	0/992
50	81.34	5/93	18/53	0/594	40/81	0/056	0.912	93/45	0/0007	0/998
75	119.1	6/88	22/51	0/681	68/8	0/058	0.904	136/9	0/0005	0/993
100	155.1	9/41	25/18	0/774	111/5	0/061	0.876	185/1	0/0003	0/994

driven by the large concentration gradients of the TC [50]. The second gentle stage illustrated the gradual decrease of adsorption rates until reaching equilibrium stage due to the low residual concentrations of adsorbate in the solution, and a small amount of active binding sites remained on the MIP surface in which IPD of the TC into pores of the MIP started to become the rate-limiting step [51]. Thus, the overall adsorption of TC by the MIP was jointly controlled by IPD and external mass transfer.

3.6. Effect of temperature and thermodynamic study

The effect of temperature (20°C–50°C) on TC adsorption was evaluated at pH of 5, initial TC concentration of 100 mg/L, and MIP mass 0.6 g/L, and the results are shown in Fig. 12. It can be seen that by increasing the temperature from 20°C to 50°C, the adsorption capacity was increased from 148.5 to 165.5 mg/g.

This could be as a result of the increase in kinetic effect, thus leading to increased mobility of the adsorbates molecule as temperature increased [52]. The high adsorption recorded indicates the process is endothermic. A further increase in temperature beyond 30°C had an insignificant effect. The removal percentage of increased gradually to reach the percentage removal of 99.57% at 50°C.

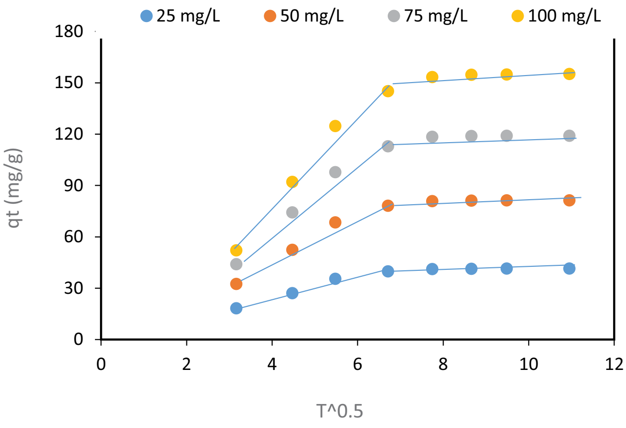

Fig. 11. Intra-particle diffusion kinetic plots for adsorption of TC onto MIP.

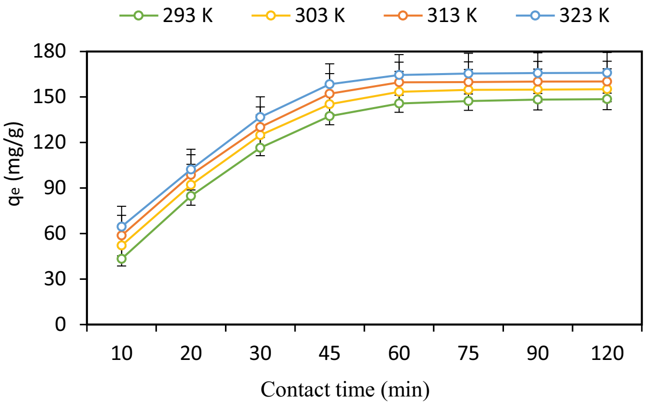

Fig. 12. Effect of temperature on TC removal (pH = 5, MIP mass 0.6 g/L, and C_0 = 100 mg/L).

Thermodynamic parameters such as standard Gibbs free energy change ($\Delta G°$), enthalpy change ($\Delta H°$), and entropy change ($\Delta S°$) at equilibrium at different temperatures can be calculated from the Langmuir isotherm equation as the following equations [53,54]:

$$\Delta G° = -RT \ln K \tag{12}$$

$$\ln K_0 = \frac{\Delta S°}{R} - \frac{\Delta H°}{RT} \tag{13}$$

where K (L/mol) is the Langmuir constant. Thermodynamic conditions will give more information on the reaction mechanism and sorption process (Table 4). The value of $\Delta H°$ change is positive, which indicates an endothermic process. The enthalpy of TC onto MIP are 41.75 kJ/mol. This suggests that the interaction of TC ions with MIP is endothermic [55]. The value of $\Delta S°$ is positive (0.195 kJ/mol K). This signifies a strong affinity of ions for adsorbents and a high degree of randomness [56]. The value of $\Delta G°$ is negative (–15.37 to –21.26), and it measures the spontaneity of a reaction process. From Table 4, it can be seen that as temperature increased from 293 to 323 K, the free energy increased (become more negative). This indicates a favorable and energetically spontaneous reaction [57]. The analysis shows the process was characterized by high randomness and spontaneous endothermic.

3.7. Regeneration and reuse of the adsorbent

The feasibility of reusing an adsorbent is correlated to its regeneration capacity. It is an important aspect of the economic perspective of the operation by enabling the prolonged use of the material [58]. The potential for regeneration and proposed reuse for the adsorbent was explored for six consecutive cycles. Fig. 13 shows the behavior of the adsorption capacity of the MIP during each of the adsorption/regeneration cycles. According to the results, it can be observed that the material preserved its adsorptive capacity in the first two cycles of use. From the first use (153.4 mg/g) to the sixth reuse (140.6 mg/g), and the capacity reduction was approximately 8.3%. Therefore, these results indicate that the MIP, besides being efficient in removing TC in an aqueous solution, is also viable in reusing and maintaining a remarkable adsorption capacity at least six regeneration cycles.

Table 4
Values of thermodynamic parameters for the adsorption of TC onto MIP

Temperature (k)	$\Delta G°$ (kJ/mol)	$\Delta H°$ (KJ/mol)	$\Delta S°$ (kJ/mol K)
293	–15.37	41.75	0.195
303	–17.53		
313	–19.33		
323	–21.26		

3.8. Competitive adsorption experiments

For conducting competitive adsorption experiments, MIP (0.6 g/L) was poured into a mixed solution containing TC, ciprofloxacin (CIP), and amoxicillin (AMO) ions. The related experiments were carried out using individual concentrations of 100 mg/L, pH of 5, the temperature of under 303 K, and contact time of 60 min. Using Eq. (14), the selectivity coefficient (*K*) was calculated [59]:

$$K = \frac{q_x / q_a}{C_x / C_a} \tag{14}$$

In Eq. (15), the adsorption capacity of *X* ions in the mixed solution has been shown q_x (mg/g); q_a (mg/g) is indicative of the total adsorption capacity of the rest of the ions in the mixed solution, C_x (mg/g) represents the initial concentration of *X* ions in the mixed solution, and C_a (mg/g) is the initial concentration of the rest of the ions in the mixed solution.

The results related to the adsorption capacity of the MIP for TC, CIP, and AMO ions at different times have been reported in Fig. 14. The order of adsorption capacity of the tested ions was detected as follows: TC > CIP > AMO; this indicative of a high adsorption selectivity for TC on MIP. Moreover, *K* values observed for the adsorbents to TC can attain about 2.96 in 60 min; this value was 2.5 times higher to compared values obtained for CIP and 3.4 times greater to values compared to AMO. Choosing TC removal in the presence of competitive ions may be due to two possible reasons; one of these reasons may be related to the size of TC, which is exactly equal to the cavities of the MIP [60]. Another reason may be described by the coordination geometry selectivity, which may play an imperative role since the ligand groups are organized by the TC-MIP sorbent in a way, which is essential for the suitable coordination of TC. In other words, the detected imprinting effect is governed by the shape and functionality of the imprinting template. Thus, according to the results, it can be concluded that the selective separation of TC by imprinted sorbent is successfully possible even in the presence of other ions [35].

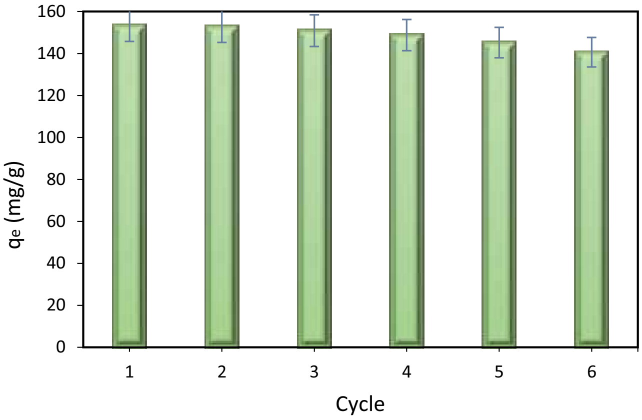

Fig. 13. Adsorption/regeneration cycles for MIP (pH = 5, MIP mass 0.6 g/L, and C_0 = 100 mg/L).

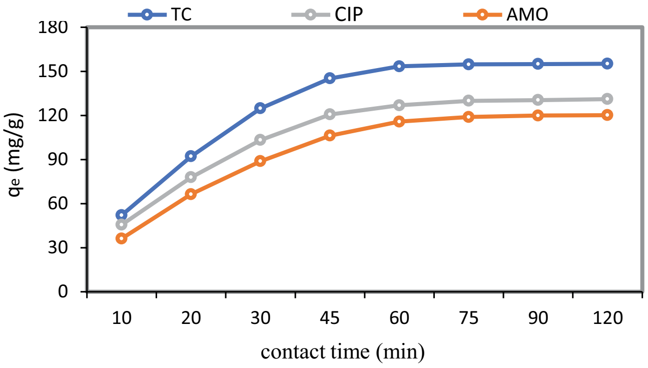

Fig. 14. Comparison of adsorption capacity of TC, CIP, and AMO ions on MIP (pH = 5, dosage = 0.6 g/L, *T* = 303 K, and individual ion concentration = 100 mg/L).

4. Conclusion

The MIP was successfully prepared by a one-pot bulk polymerization method and used in the removal of TC from aqueous environments. MIP specifications were determined using XRD, TGA, SEM, and BET analysis. The results revealed that the removal percentage of TC onto MIP was enhanced with increasing contact time, temperature, and MIP dose, but it was also reduced with increasing initial concentration and solution pH. The proposed MIP exhibited a rapid adsorption rate (60 min) and high adsorption capacity. In the adsorption isotherm, the Langmuir model was best fitted with the experimental data indicating the homogeneous nature of binding sites in the adsorbent. The PSO equation was found to be the best-fitting model for the experimental data of TC ions adsorption. The thermodynamic parameters indicated that the adsorption process was spontaneous and endothermic. The MIP may be used as an effective adsorbent for the selective uptake of TC ions from the aqueous solutions.

Acknowledgments

The authors are grateful to the Zahedan University of Medical Sciences for the financial support of this study.

References

[1] R. Rostamian, H. Behnejad, A comparative adsorption study of sulfamethoxazole onto graphene and graphene oxide nanosheets through equilibrium, kinetic and thermodynamic modeling, Process Saf. Environ. Prot., 102 (2016) 20–29.
[2] R. Diyanati, J. Yazdani, Effect of sorbitol on phenol removal rate by *Lemna minor*, J. Mazandaran Univ. Med. Sci., 22 (2013) 58–65.
[3] D. Balarak, F.K. Mostafapour, Photocatalytic degradation of amoxicillin using UV/synthesized NiO from pharmaceutical wastewater, Indonesian J. Chem., 19 (2019) 211–218.
[4] Y.X. Song, S. Chen, N. You, H.T. Fan, L.N. Sun, Nanocomposites of zero valent iron-activated carbon derived from corn stalk for adsorptive removal of tetracycline antibiotics, Chemosphere, 225 (2020) 1–10, doi: 10.1016/j.chemosphere.2020.126917.
[5] S. Ahmadi, A. Banach, F.K. Mostafapour, Study survey of cupric oxide nanoparticles in removal efficiency of ciprofloxacin antibiotic from aqueous solution: adsorption isotherm study, Desal. Water Treat., 89 (2017) 297–303.

[6] P. Rajiv, N. Mengelizadeh, G. McKay, Photocatalytic degradation of ciprofloxacin with Fe_2O_3 nanoparticles loaded on graphitic carbon nitride: mineralisation, degradation mechanism and toxicity assessment, Int. J. Environ. Anal. Chem., (2021), doi: 10.1080/03067319.2021.1890059.

[7] D. Balarak, H. Azarpira, F.K. Mostafapour, Adsorption isotherm studies of tetracycline antibiotics from aqueous solutions by maize stalks as a cheap biosorbent, Int. J. Pharm. Technol., 8 (2016) 16664–16675.

[8] A.H. Mahvi, F.K. Mostafapour, Biosorption of tetracycline from aqueous solution by *Azolla filiculoides*: equilibrium kinetic and thermodynamics studies, Fresenius Environ. Bull., 27 (2018) 5759–5767.

[9] Z. Zhang, H. Li, H. Liu, Insight into the adsorption of tetracycline onto amino and amino-Fe^{3+} functionalized mesoporous silica: effect of functionalized groups, J. Environ. Sci., 65 (2018) 171–178.

[10] J.M. Lv, Y.L. Ma, X. Chang, S.B. Fan, Removal and removing mechanism of tetracycline residue from aqueous solution by using Cu-13X, Chem. Eng. J., 273 (2015) 247–253.

[11] J. Cao, Z. Xiong, B. Lai, Effect of initial pH on the tetracycline (TC) removal by zero-valent iron: adsorption, oxidation and reduction, Chem. Eng. J., 343 (2018) 492–499.

[12] R. Acosta, V. Fierro, A.M. Yuso, D. Nabarlatz, A. Celzard, Tetracycline adsorption onto activated carbons produced by KOH activation of tyre pyrolysis char, Chemosphere, 149 (2016) 168–176.

[13] A.C. Martins, O. Pezoti, A.L. Cazetta, K.C. Bedin, D.A.S. Yamazaki, Removal of tetracycline by NaOH-activated carbon produced from macadamia nut shells: kinetic and equilibrium studies, Chem. Eng. J., 260 (2015) 291–299.

[14] T.J. Al-Musawi, A.H. Mahvi, A.D. Khatibi, Effective adsorption of ciprofloxacin antibiotic using powdered activated carbon magnetized by iron(III) oxide magnetic nanoparticles, J. Porous Mater., 28 (2021) 835–852.

[15] N. You, S. Chen, Y. Wang, H.T. Fan, L.N. Sun, T. Sun, *In situ* sampling of tetracycline antibiotics in culture wastewater using diffusive gradients in thin films equipped with graphene nanoplatelets, Environ. Res., 191 (2020) 1–9, doi: 10.1016/j.envres.2020.110089.

[16] D. Balarak, F.K. Mostafapour, E. Bazrafshan, A.S. Tawfik, Studies on the adsorption of amoxicillin on multi-wall carbon nanotubes, Water Sci. Technol., 75 (2017) 1599–1606.

[17] O.K. Kuyumcu, S.S. Bayazit, M.A. Salam, Antibiotic amoxicillin removal from aqueous solution using magnetically modified graphene nanoplatelets, J. Ind. Eng. Chem., 35 (2016) 225–234.

[18] N. You, H. Yao, Y. Wang, H.T. Fan, C.S. Wang, T. Sun, Development and evaluation of diffusive gradients in thin films based on nano-sized zinc oxide particles for the *in situ* sampling of tetracyclines in pig breeding wastewater, Sci. Total Environ., 651 (2019) 1653–1660.

[19] D. Balarak, A.H. Mahvi, M.J. Shim, S.M. Lee, Adsorption of ciprofloxacin from aqueous solution onto synthesized NiO: isotherm, kinetic and thermodynamic studies, Desal. Water Treat., 212 (2021) 390–400.

[20] H.R. Pouretedal, N. Sadegh, Effective removal of amoxicillin, cephalexin, tetracycline and penicillin G from aqueous solutions using activated carbon nanoparticles prepared from vine wood, J. Water Process Eng., 1 (2014) 64–73.

[21] S.J. Zou, B.H. Ding, Y.F. Chen, H.T. Fan, Nanocomposites of graphene and zirconia for adsorption of organic-arsenic drugs: performances comparison and analysis of adsorption behavior, Environ. Res., 101 (2021) 1–12, doi: 10.1016/j.envres.2021.110752.

[22] S.T. Danalıoğlu, S.S. Bayazit, O.K. Kuyumcu, M.A. Salam, Efficient removal of antibiotics by a novel magnetic adsorbent: magnetic activated carbon/chitosan (MACC) nanocomposite, J. Mol. Liq., 240 (2017) 589–596.

[23] L. Huang, M. Wang, C. Shi, J. Huang, B. Zhang, Adsorption of tetracycline and ciprofloxacin on activated carbon prepared from lignin with H_3PO_4 activation, Desal. Water Treat., 52 (2014) 2678–2687.

[24] L. Madikizela, N. Tavengwa, V. Pakade, Molecularly Imprinted Polymers for Pharmaceutical Compounds: Synthetic Procedures and Analytical Applications, N. Cankaya, Ed., Recent Research in Polymerization, IntechOpen, 2018, pp. 1–22. Available at: https://www.intechopen.com/books/recent-research-in-polymerization/molecularly-imprinted-polymers-for-pharmaceutical-compounds-synthetic-procedures-and-analytical-appl

[25] W. Lu, J. Liu, J. Li, X. Wang, M. Lv, R. Cui, L. Chen, Dual-template molecularly imprinted polymers for dispersive solid-phase extraction of fluoroquinolones in water samples coupled with high performance liquid chromatography, Analyst, 144 (2019) 1292–1302.

[26] X. Sun, J. Wang, Y. Li, J. Yang, J. Jin, S.M. Shah, J. Chen, Novel dummy molecularly imprinted polymers for matrix solid-phase dispersion extraction of eight fluoroquinolones from fish samples, J. Chromatogr. A, 1359 (2014) 1–7.

[27] L.F. Miranda, D.S. Domingues, M.E. Queiroz, Selective solid-phase extraction using molecularly imprinted polymers for analysis of venlafaxine, odesmethylvenlafaxine, and N-desmethylvenlafaxine in plasma samples by liquid chromatography-tandem mass spectrometry, J. Chromatogr. A, 1458 (2016) 46–53.

[28] C. Cacho, E. Turiel, C.P. Conde, Molecularly imprinted polymers: an analytical tool for the determination of benzimidazole compounds in water samples, Talanta, 78 (2009) 1029–1035.

[29] R.R. Pupin, M.V. Foguel, L.M. Gonçalves, M.P.T. Sotomayor, Magnetic molecularly imprinted polymers obtained by photopolymerization for selective recognition of penicillin G, J. Appl. Polym. Sci., 137 (2019) 1–10.

[30] D.A. Spivak, Optimization, evaluation, and characterization of molecularly imprinted polymers, Adv. Drug Deliv. Rev., 57 (2005) 1779–1794.

[31] P.A. Cormack, A.Z. Elorza, Molecularly imprinted polymers: synthesis and characterisation, J. Chromatogr. B, 804 (2004) 173–182.

[32] Z. Meng, W. Chen, A. Mulchandani, Removal of estrogenic pollutants from contaminated water using molecularly imprinted polymers, Environ. Sci. Technol., 39 (2005) 8958–8962.

[33] M. Li, D. Shu, L. Jiang, Cu(II)-influenced adsorption of ciprofloxacin from aqueous solutions by magnetic graphene oxide/nitrilotriacetic acid nanocomposite: competition and enhancement mechanisms, Chem. Eng. J., 319 (2017) 219–228.

[34] H. Peng, B. Pan, M. Wu, Y. Liu, D. Zhang, B. Xing, Adsorption of ofloxacin and norfloxacin on carbon nanotubes: hydrophobicity and structure-controlled process, J. Hazard. Mater., 233–234 (2012) 89–96.

[35] Y. Lin, S. Xu, L. Jia, Fast and highly efficient tetracyclines removal from environmental waters by graphene oxide functionalized magnetic particles, Chem. Eng. J., 225 (2013) 679–685.

[36] G. Li, D. Zhang, M. Wang, J. Huang, L. Huang, Preparation of activated carbons from Iris tectorum employing ferric nitrate as dopant for removal of tetracycline from aqueous solutions, Ecotoxicol. Environ. Saf., 98 (2013) 273–282.

[37] F. Güzel, H. Sayğılı, Adsorptive efficacy analysis of novel carbonaceous sorbent derived from grape industrial processing wastes towards tetracycline in aqueous solution, J. Taiwan Inst. Chem., 60 (2016) 236–240.

[38] Y. Gao, Y. Li, L. Zhang, H. Huang, J. Hu, S.M. Shah, X. Su, Adsorption and removal of tetracycline antibiotics from aqueous solution by graphene oxide, J. Colloid Interface Sci., 368 (2012) 540–546.

[39] L. Ji, W. Chen, L. Duan, D. Zhu, Mechanisms for strong adsorption of tetracycline to carbon nanotubes: a comparative study using activated carbon and graphite as adsorbents, Environ. Sci. Technol., 43 (2018) 2322–2327.

[40] J.R. Utrilla, C.V.G. Pacheco, M.S. Polo, J.J.L. Peñalver, R.O. Pérez, Tetracycline removal from water by adsorption/bioadsorption on activated carbons and sludge-derived adsorbents, J. Environ. Manage., 131 (2013) 16–24.

[41] Z. Li, P.H. Chang, J.S. Jean, W.T. Jiang, C.J. Wang, Interaction between tetracycline and smectite in aqueous solution, J. Colloid Interface Sci., 341 (2010) 311–319.

[42] N. You, X.F. Wang, J.Y. Li, H.T. Fan, H. Shen, Q. Zhang, Synergistic removal of arsanilic acid using adsorption and magnetic separation technique based on Fe_3O_4@graphene nanocomposite, J. Ind. Eng. Chem., 70 (2019) 346–354.

[43] Z. Li, L. Schulz, C. Ackley, N. Fenske, Adsorption of tetracycline on kaolinite with pH-dependent surface charges, J. Colloid Interface Sci., 351 (2010) 254–260.

[44] P.H. Chang, Z. Li, W.T. Jiang, J.S. Jean, Adsorption and intercalation of tetracycline by clay minerals, Appl. Clay Sci., 46 (2009) 27–36.

[45] P.H. Chang, Z. Li, T.L. Yu, S. Munkhbayer, T.H. Kuo, Y.C. Hung, J.S. Jean, Sorptive removal of tetracycline from water by palygorskite, J. Hazard. Mater., 165 (2009) 148–155.

[46] M.H. Marshal, M. Esmaieli, H. Abolghasemi, M.H. Marzbali, Tetracycline adsorption by H_3PO_4-activated carbon produced from apricot nut shells: a batch study, Process Saf. Environ. Prot., 102 (2016) 700–709.

[47] M.B. Ahmed, J.L. Zhou, H.H. Ngo, Adsorptive removal of antibiotics from water and wastewater: progress and challenges, Sci. Total Environ., 532 (2015) 259–268.

[48] Y. Zhang, Z. Jiao, Y. Hu, S. Lv, H. Fan, Y. Zeng, Removal of tetracycline and oxytetracycline from water by magnetic Fe_3O_4 graphene, Environ. Sci. Pollut. Res., 15 (2016) 1–9.

[49] X. Ren, C. Chen, M. Nagatsu, X. Wang, Carbon nanotubes as adsorbents in environmental pollution management: a review, Chem. Eng. J., 170 (2011) 395–410.

[50] L. Ji, Y. Shao, Z. Xu, S. Zheng, D. Zhu, Adsorption of monoaromatic compounds and pharmaceutical antibiotics on carbon nanotubes activated by KOH etching, Environ. Sci. Technol., 44 (2010) 6429–6436.

[51] D. Balarak, H. Azarpira, F.K. Mostafapour, Study of the adsorption mechanisms of cephalexin on to *Azolla filiculoides*, Pharm. Chem., 8 (2016) 114–121.

[52] S. Li, X. Zhang, Y. Huang, Zeolitic imidazolate framework-8 derived nanoporous carbon as an effective and recyclable adsorbent for removal of ciprofloxacin antibiotics from water, J. Hazard. Mater., 321 (2017) 711–719.

[53] N. You, Y.X. Song, H.R. Wang, L.X. Kang, H.T. Fan, Sol–gel derived Benzo–Crown ether-functionalized silica gel for selective adsorption of Ca^{2+} ions, J. Chem. Eng. Data, 64 (2019) 1378–1384.

[54] F. Wang, B. Yang, H. Wang, Q. Song, F. Tan, Y. Cao, Removal of ciprofloxacin from aqueous solution by a magnetic chitosan grafted graphene oxide composite, J. Mol. Liq., 222 (2016) 188–194.

[55] S.X. Zha, Y. Zhou, X. Jin, Z. Chen, The removal of amoxicillin from wastewater using organobentonite, J. Environ. Manage., 129 (2013) 569–576.

[56] U.A. Guler, M. Sarioglu, Removal of tetracycline from wastewater using pumice stone: equilibrium, kinetic and thermodynamic studies, J. Environ. Health. Sci. Eng., 12 (2014) 79–87.

[57] H. Azarpira, Y. Mahdavi, O. Khaleghi, Thermodynamic studies on the removal of metronidazole antibiotic by multi-walled carbon nanotubes, Pharm. Lett., 8 (2016) 107–113.

[58] F. Yu, Y. Li, S. Han, Adsorptive removal of antibiotics from aqueous solution using carbon materials, Chemosphere, 153 (2016) 365–385.

[59] D. Balarak, G. McKay, Utilization of MWCNTs/Al_2O_3 as adsorbent for ciprofloxacin removal: equilibrium, kinetics and thermodynamic studies, J. Environ. Sci. Health, Part A: Toxic/Hazard. Subst. Environ. Eng., 56 (2021) 324–333.

[60] D. Balarak, Z. Taheri, M.J. Shim, S.M. Lee, C. Jeon, Adsorption kinetics and thermodynamics and equilibrium of ibuprofen from aqueous solutions by activated carbon prepared from *Lemna minor*, Desal. Water Treat., 215 (2021) 183–193.